25th ABCM International Congress of Mechanical Engineering
October 20-25, 2019, Uberlândia, MG, Brazil

COB-2019-2139
NUMERICAL CONVECTIVE MODEL FOR INTERDENDRITIC LIQUID IN A Sn - 39.5 wt% Bi SOLIDIFICATION EXPERIMENT

Leonardo Maximino Bernardo
Programa de Pós-Graduação em Ciência e Engenharia de Materiais/UFPB
lmbernardo752011@gmail.com

Romulo Heringer
Universidade Federal de Santa Catarina
romulo.heringer@ufsc.br

Abstract. *The present contribution is a numerical simulation of heat, solute and momentum balance for a interdendritic liquid region during solidification of a binary alloy. The control volume is considered in such a way that the control surface coincide with the phase change interface. As a consequence, the solid phase surrounds our system and solute segregation is considered as flux through the frontier, handled via boundary condition. An special case is studied, where the growth direction of columnar structures is not aligned with thermal gradient. The aim of present work was to verify if solutal and thermal convection in a confined interdendritic region can affect both: a) the local solid fraction evolution; b) the asymmetry observed on the growth of dendrite secondary arms in some alloys, which are longer in the side exposed to higher temperatures.*

Keywords: *solidification, segregation, thermal and solutal convection.*

1. INTRODUCTION

In a recent experiment, Gibbs *et al.* (2016) used *in-situ* X-ray radiography through a thin Sn - 39.5 wt% Bi sample, to take a set of images of microstructures growing during directional bottom-up solidification of the alloy. Their main objective was to count the fragmentation events in the mushy zone. In this context, fragmentation is the breaking of dendrite arms associated with diffusion caused by differences on the curvature of solid liquid interface. This phenomenon is believed to be the origin of spontaneous grain refining (Herlach (1994)).

The present authors, in a previous investigation, realized an attempt to evaluate the probable causes of a non-monotonic behavior of the averaged solid fraction in the visible region on the experiment of Gibbs *et al.* (2016). This was done by a diffusive model, which results showed no remelting. The objective of the present analysis is to include convection effect in the studied process, which was not considered in the diffusive model.

The effect of convestion on solidification rate and dendrite growth kinetics has experienced considerable progress. Wang and Beckermann (1996) investigated equiaxed dendritic solidification in the presence of melt convection and solid-phase transport in a series of three articles. Beckermann (1997) summarized some advances in modelling solute redistribution and grain structure formation in purely equiaxed alloy solidification giving emphasis on the influence of convection.

In the present work we consider a convection caused by segregation in a confined interdendritic region. This is a likely approach, regarded the specific experimental conditions of Gibbs *et al.* (2016), where the sample thickness is of the order of microstrucutres, confined between crucible plates.

2. CONVECTIVE MODEL FOR A CONFINED INTERDENDRITIC REGION

Our analysis is restricted to the control volume, consisting of a rectangular area of $175 \times 100\,\mu$m was as shown in Fig. 1. The control volume was considered as the interdendritic liquid surrounded by solidified alloy, so that the control surface coincide with the solid-liquid phase change interface. The boundaries of this system was considered to coincide with the solid liquid interface on all sides. In this way the system always consists of liquid in phase change, while the surround is the solid phase. As a major simplification, the control surface is static, that is, the physical solid liquid interface is represented only by an abstract kinetic and by a solute flux, segregated from surrounds to the liquid in the control volume trough the boundaries. The mathematical

position of that interface does not change.

This present model was developed to calculate the conservation equation for the thermal energy, the solute mass concentration and linear momentum of alloy solute.

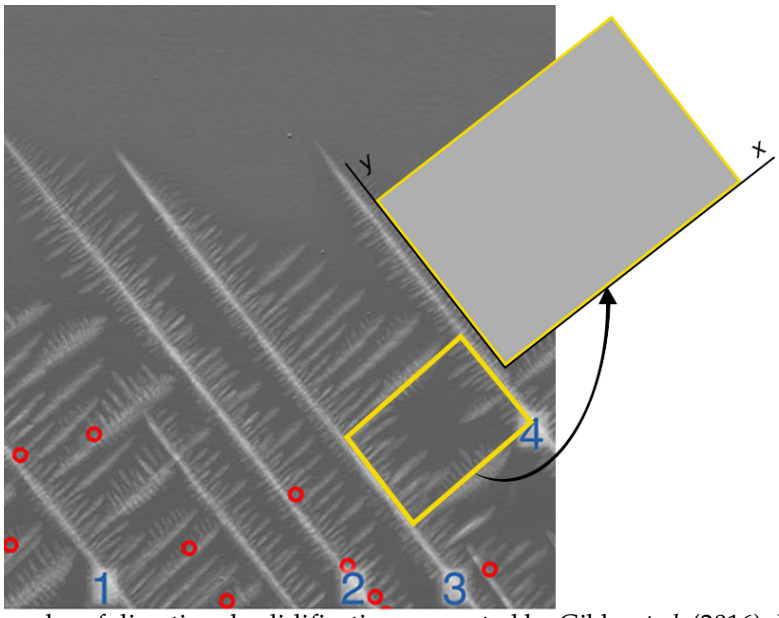

Figure 1: X-ray radiography of directional solidification presented by Gibbs *et al.* (2016). Fragmentation events were highlighted with red circles. The rectangle corresponds to the choice of control volume used in the present work.

2.1 Heat transfer

The volume of rectangular control highlighted in the Fig. 1 is subject to a temperature distribution given by this gradient along the volume of control that is certainly solidifying. The thermal energy conservation equation is:

$$\frac{\partial T}{\partial t} + \boldsymbol{\nabla}.(\boldsymbol{u}\,T) - \boldsymbol{\nabla}\cdot(\alpha_T\,\boldsymbol{\nabla}T) = S_T \tag{1}$$

In this text, bold face mathematical symbols indicate vectors.

The initial condition for the temperature is:

$$T(x,y,t=0) = T(x=0,y=0,t=0)_{Ref} + \boldsymbol{\nabla}T\cdot\boldsymbol{r} \tag{2}$$

Where $T(0,0,0)_{Ref}$ is the temperature imposed at time $t = 0\,\text{s}$, chosen in such a way that the maximum system temperature (upper right corner of the control volume) starts as the *liquidus* temperature, related to the nominal composition of the alloy. $\boldsymbol{\nabla}T$ is the vector temperature gradient, known from the experiment information, $\boldsymbol{r}$ is the position vector. The boundary conditions for the thermal problem are:

$$\frac{\partial T}{\partial y} = -2200.0;\ \text{para:}y = 0; \tag{3}$$

$$\frac{\partial T}{\partial y} = 2200.0;\ \text{para:}y = 100\,\mu\text{m}; \tag{4}$$

$$\frac{\partial T}{\partial x} = -1810.7;\ \text{para}: x = 0; \tag{5}$$

$$\frac{\partial T}{\partial x} = 1810.7;\ \text{para}: x = 175\,\mu\text{m}. \tag{6}$$

2.2 Source of thermal energy due to solidification

In the Eq. (1) the enthalpy of fusion released is taken into account through the term S_T. This term is given by

$$S_T = \frac{L_f}{\rho\, c_p}\,\frac{dg_s}{dt}. \tag{7}$$

Where, L_f is the enthalpy of fusion, c_p is the alloy specific heat

2.3 Solute transfer

The solute conservation equation can be written as follows (Dantzig and Rappaz (2009))

$$\frac{\partial w}{\partial t} + \boldsymbol{\nabla}\cdot(\boldsymbol{u}w) - \boldsymbol{\nabla}\cdot(D\boldsymbol{\nabla}w) = 0 \tag{8}$$

In this equation, D is the diffusion coefficient of the solute in the solvent. The initial condition for the solute field was obtained considering the concentration equivalent to the liquidus line for the initial temperature at each point. That is,

$$w(x,y,t=0) = \frac{1}{m}\,\left[T_{liquidus}(x,y,t=0) - T_f\right] \tag{9}$$

Segregation of solute from the solid to the liquid through the solidification interface is carried out through the boundary conditions:

$$\frac{\partial w}{\partial x} = \frac{1}{D\,S_v}\,\frac{dg_s}{dt}\,w;\ \text{para:}y = 0; \tag{10}$$

$$\frac{\partial w}{\partial x} = \frac{1}{D\,S_v}\,\frac{dg_s}{dt}\,w;\ \text{para:}y = 100\,\mu\text{m}; \tag{11}$$

$$\frac{\partial w}{\partial y} = \frac{1}{D\,S_v}\,\frac{dg_s}{dt}\,w;\ \text{para}: x = 0; \tag{12}$$

$$\frac{\partial w}{\partial y} = \frac{1}{D\,S_v}\,\frac{dg_s}{dt}\,w;\ \text{para}: x = 175\,\mu\text{m}. \tag{13}$$

Here, S_v is the magnitude of $\boldsymbol{s_v}$, which is the vector of phase change surface density defined as $\boldsymbol{s}_v \equiv \dfrac{\hat{\boldsymbol{n}}\,S}{V}$. For a partition of control volume closed to the boundary, the surface density vector is defined as the ratio between the partition volume and the part of partition surface lying on that boundary, that is, the phase change interface area in the present context.

2.4 Initial undecooling and *liquidus* temperature

The solid and liquid temperatures at the interface must be equal under the thermodynamic equilibrium condition $T_l = T_s = T_{liquidus}$, the temperature at the interface. We will take the linear fitting of the *liquidus* line from the phase diagram of the concerned alloy.

$$T_{liquidus}\,(x,y,t) = T_f + m\,w \tag{14}$$

With T_f being the melting temperature for the linear adjustment of the *liquidus* line and m the slope coefficient. Calculating the temperature *liquidus* equivalent to the concentration of the liquid near the limit, the undercooling necessary to obtain the solidification velocity is calculated as

$$\Delta T = T_{liquidus} - T. \tag{15}$$

2.5 Growth kinetics

Let $\boldsymbol{\mathcal{V}}^*$ be the velocity of solidification front. This front is a imaginary surface touching the dendrite tips, defining a solid liquid region (mushy zone) from the bulk liquid. By doing so, the front velocity is the dendrite growth rate. Several models have been developed for dendrite growth Kurz and Fisher (1989). In the present case, calculation of front velocity was based on that of Lipton *et al.* (1984). However, following an usual approach in numerical solidification simulation, it was adopted a simplified model for calculating $\boldsymbol{\mathcal{V}}^*$, which

consists of a curve fitting obtained using more elaborated models for dendritic growth kinetics. From the results of growth models, a curve fitting is performed to obtain a more convenient form, where $\boldsymbol{\mathcal{V}}^*$ depends on a single parameter: the ΔT undercooling. Typically, the results are as follow (Heringer, 2004),

$$\boldsymbol{\mathcal{V}}^* = \mathcal{A}\,(\Delta T)^{\mathcal{N}}\,\hat{\boldsymbol{n}}. \tag{16}$$

$\mathcal{A}$ and $\mathcal{N}$ are constants obtained from the quoted fitting. By definition, $\boldsymbol{\mathcal{V}}^*$ is always orthogonal to the solidification interface and therefore orthogonal to the control volume boundary as defined in the present model. Therefore, $\hat{n}$ is a unit vector normal to the solid/liquid interface.

2.6 Solidification rate

In this paragraph we can deal with the scalar $\mathcal{V}^* = \boldsymbol{\mathcal{V}}^* \cdot \hat{\boldsymbol{n}}$, where $\hat{\boldsymbol{n}}$ is the normal unit vector defined on a surface point. That said, if S is the solid/liquid interface area, the volume growth rate of solid is

$$\frac{dV_s}{dt} \;=\; \mathcal{V}^*\,S. \tag{17}$$

Dividing both sides by the total volume V (which does not vary over time), and recognizing that $\dfrac{V_s}{V} = g_s$ is the solid fraction, and $\dfrac{S}{V}$ is S_v, the magnitude of $\boldsymbol{s_v}$,

$$\frac{dg_s}{dt} \;=\; \mathcal{V}^*\,S_v \tag{18}$$

The control volume was defined inside a mushy zone, so, $g_s \neq 0$ at $t = 0$. In the context of present model, since the control volume is always entirely liquid, a volumetric solid fraction g_s is not a property of the system. Despite this fact, a surrounding g_s evolution can be evaluated by integrating dg_s/dt, provided that its value is known at initial time. In the present work this value was based from experimental data from Gibbs *et al.* (2016).

2.7 Momentum conservation

The momentum conservation equation can be written for the considered system, starting from the Navier-Stokes equation assuming the following form:

$$\frac{\partial(\rho \boldsymbol{u})}{\partial t} + \boldsymbol{\nabla}.(\rho \boldsymbol{u}\boldsymbol{u}) = -\boldsymbol{\nabla} p + \mu \nabla^2 \boldsymbol{u} + \rho_0\, \boldsymbol{g}\;\left[\beta_T\left(T - T_{ref}\right) - \beta_c\left(w - w_{ref}\right)\right] \tag{19}$$

Where the Boussinesq approximation was applied. The terms, β_T and β_c, ρ_0, T_{ref} and w_{ref}, are, respectively, the coefficients of thermal and solute expansion, the density, temperature and mass concentration references. As initial condition, velocity was zero in the control volume, that is,

$$\boldsymbol{u}(x, y, t = 0) = 0. \tag{20}$$

The boundary conditions for the linear momentum transport are:

$$\boldsymbol{u} = 0;\;\; \text{para} : y = 0; \tag{21}$$
$$\boldsymbol{u} = 0;\;\; \text{para} : y = 100\,\mu\text{m}; \tag{22}$$
$$\boldsymbol{u} = 0;\;\; \text{para} : x = 0; \tag{23}$$
$$\boldsymbol{u} = 0;\;\; \text{para} : x = 175\,\mu\text{m}. \tag{24}$$

The model presented in the previous section describes the movement, heat transfer and solute in the liquid medium that make up the control volume in the present case.

3. NUMERICAL APPROACH

The set of coupled differential balance equations has been solved using the finite volume method. The control volume had been partitioned using a structured uniform mesh with 200×200 nodes.

In summary, the following algorithm had been proposed to solve mathematical model:

1. Setup of initial values for all fields;
2. Increasing time ($t + \Delta t$);
3. Velocity field calculation by solving the Navier-Stokes equation (Eq. (19));
4. Temperature field calculation (Eq. (1));
5. Calculation of solute field by solving the solute conservation equation (Eq. (8));
6. Calculation of *liquidus* temperature (Eq. (14)) and undercooling (Eq. (15));
7. Calculation of growth velocity (Eq. (16));
8. Calculation of temporal rate of change of solid fraction (Eq. (18));
9. Calculation of solid fraction by solving numerically Eq. (18) from t to $t + \Delta t$;
10. Calculation of source term for the thermal energy due to the solidification (Eq. (7));
11. Calculation of pressure field using PIMPLE algorithm (OpenFOAM (2018));
12. If fields are not converged, return to step 3; Otherwise, go to next step;
13. If time is less than end time, return to step 2; Otherwise, finish.

The above algorithm was implemented using *OpenFOAM*® library, an open source computational package written in C++, dedicated to solving problems of transport phenomena, where the differential equations are discretized according to the finite volume method.

3.1 Running conditions

The general conditions for calculating the model equations for interdendritic liquid take into account the parameters listed in Tab. 1, below:

Table 1: General conditions used in the calculus

Symbol	Description	Value [SI unit]
ν	Kinematic viscosity	2.16216×10^{-7} $\left[\mathrm{m^2 s^{-1}}\right]$
β_T	Thermal expansion coefficient	1.06×10^{-4} $\left[\mathrm{K^{-1}}\right]$
β_C	Solutal expansion coefficient	-0.172 $\left[(\mathrm{wt\%})^{-1}\right]$
D	Diffusion coefficient	$3.5 \times 10^{-9} [\mathrm{m^2 s^{-1}}]$
w_0	Nominal solute mass fraction	39.5 [wt%]
T_f	Temperature for $w = 0$ (*liquidus* line linear fitting)	528.15 [K]
m	Linear *liquidus* slope	-2.0515 [K]
κ	Thermal conductivity	24.0 $\left[\mathrm{W m^{-1} K^{-1}}\right]$
g_{s0}	Initial solid fraction	0.1 $[-]$
ΔT_0	Undercooling	0 [K]
L_f	Enthalpy of fusion	4.3106×10^8 $\left[\mathrm{J m^{-3}}\right]$
c	Specific heat	201.0 $\left[\mathrm{J kg^{-1} K^{-1}}\right]$
ρ	Density	8.325×10^3 $\left[\mathrm{K g m^{-3}}\right]$
T_E	Eutectic temperature	412.15 [K]
w_E	Eutectic composition	56 [wt%]
ΔT_E	Eutectic undercooling	2 [K]
k	Partition coefficient	0.37 $[-]$
T_{Ref}	Reference temperature	447.11 [K]
w_{Ref}	Reference solute mass fraction	39.5 [wt%]
$\frac{dT}{dt}$	Temperature ratio	-0.06033 $\left[\mathrm{K s^{-1}}\right]$
$\mathcal{A}$	Coefficient for solidification velocity	2.9×10^{-6} $\left[\mathrm{m s^{-1}}\right]$
$\mathcal{N}$	Exponent for solidification velocity	2.7 $[-]$

4. RESULTS AND DISCUSSIONS

Some examples of velocity field and streamlines are shown on Fig. 2 for qualitative evaluation. The fluid movement is of order of magnitude $10^{-6}\,\mathrm{m\,s^{-1}}$. Despite this fact, convection has an effect on solute distribution, as can be noted at the left upper corner of Fig. 3-a. Concentration field analysis of the $Sn - 39.5\,p\%\,Bi$ alloy Fig.3-a shows a higher bismuth concentration on the lower left side of the control volume. In the upper left side there is an additional accumulation due to the natural convection driven by species distribution.

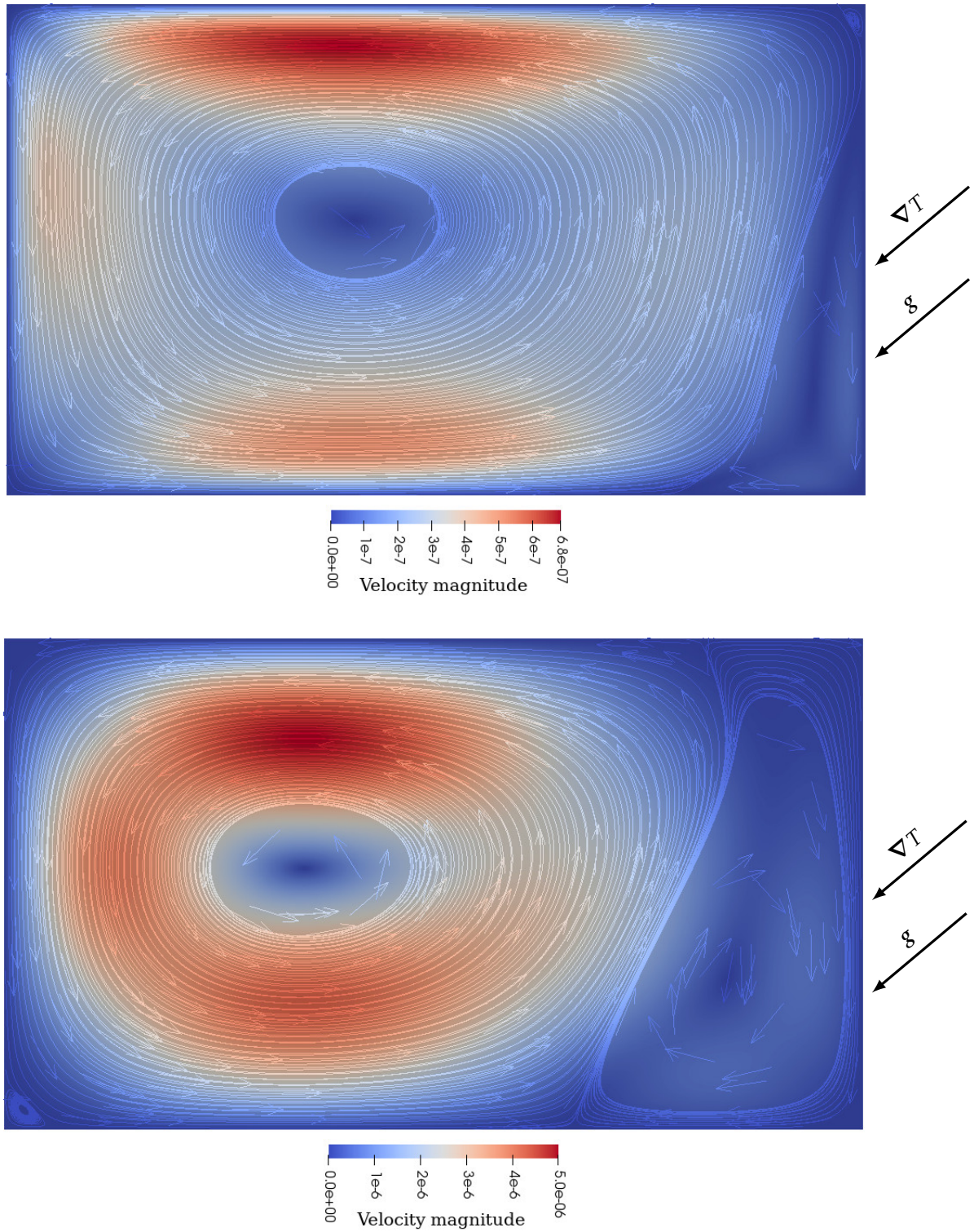

Figure 2: Velocity field for $t = 20\,\mathrm{s}$ (top) and $t = 600\,\mathrm{s}$ (bottom), in $\mathrm{m\,s^{-1}}$. The vectors next to each map are temperature gradient ($\boldsymbol{\nabla} T$) and gravity ($\boldsymbol{g}$).

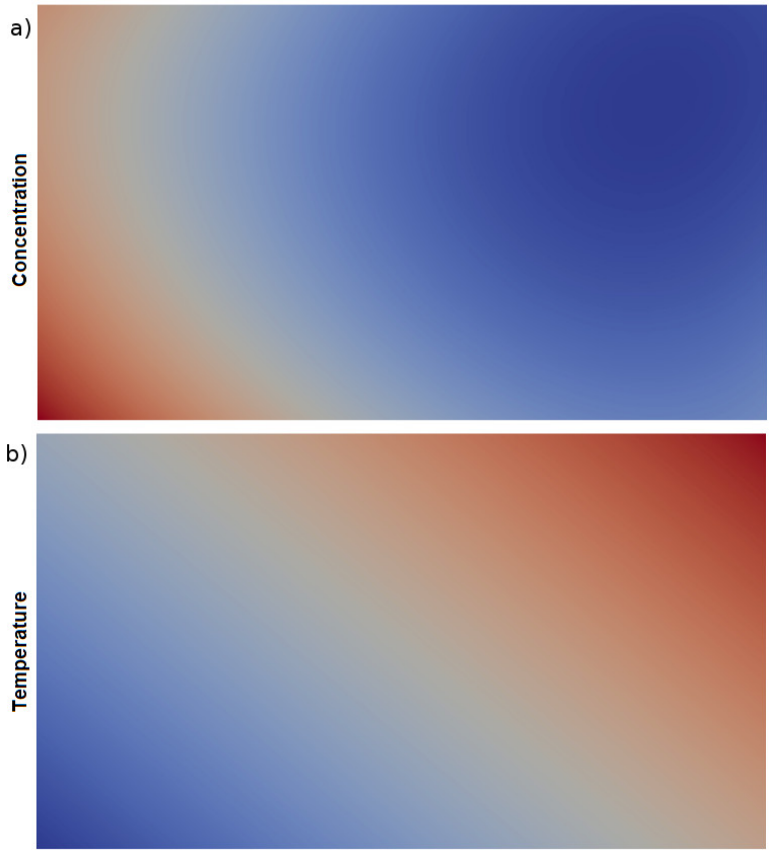

Figure 3: Fields of a) bismuth mass concentration, b) temperature.

The temperature field does not drive fluid flow, since the temperature gradient is antiparallel to the gravity vector. This convection is driven by non-uniformity in solute (Bismuth) distribution, which is caused by segregation from the solid through the liquid boundary. As expected due to milimetrical size of the control volume, although not uniform, the variation of bismuth along the liquid is very small (Fig. 4).

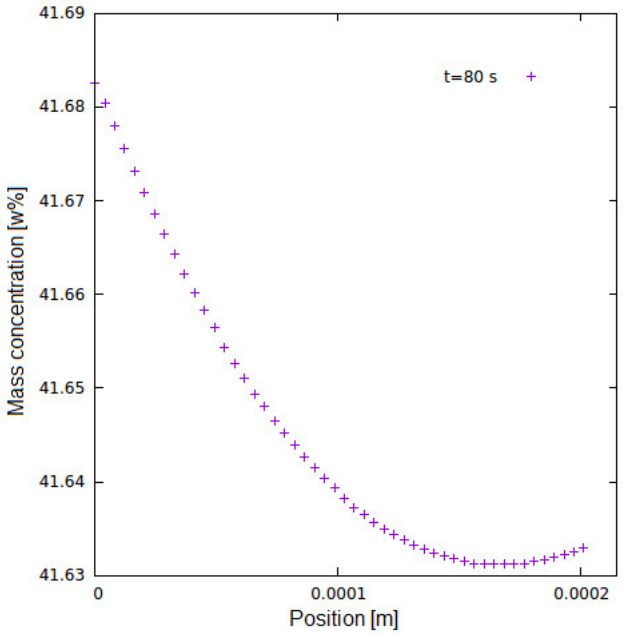

Figure 4: Solute (Bi) profile along the diagonal line (bottom-up, left to right) on the control volume, for $t = 80\,\mathrm{s}$.

Figure 5 shows the results for solid fraction evolution. It should be noted that for this case g_s does not start with zero value because the control volume consists of an interdendritic region taken in a mushy zone.

It can be observed a good agreement between experimental and numerical results, until the measured solid fraction shows a non-monotonic behavior and decreases, especially after 74 s. The present work had allowed to conclude that there is no influence of solute redistribution due to interdendritic local convection on the non monotonic behavior of solid fraction history. In fact, the solid fraction reduction saw in experimental results of Fig. 5 isn't remelting. It is rather due to buoyancy of dendrite fragments out of measure region. Gibbs *et al.* (2016) did not report this fact in their paper. This local effect isn't included in the present model. So, no comparisons can be expected after this buoyancy effect becomes important.

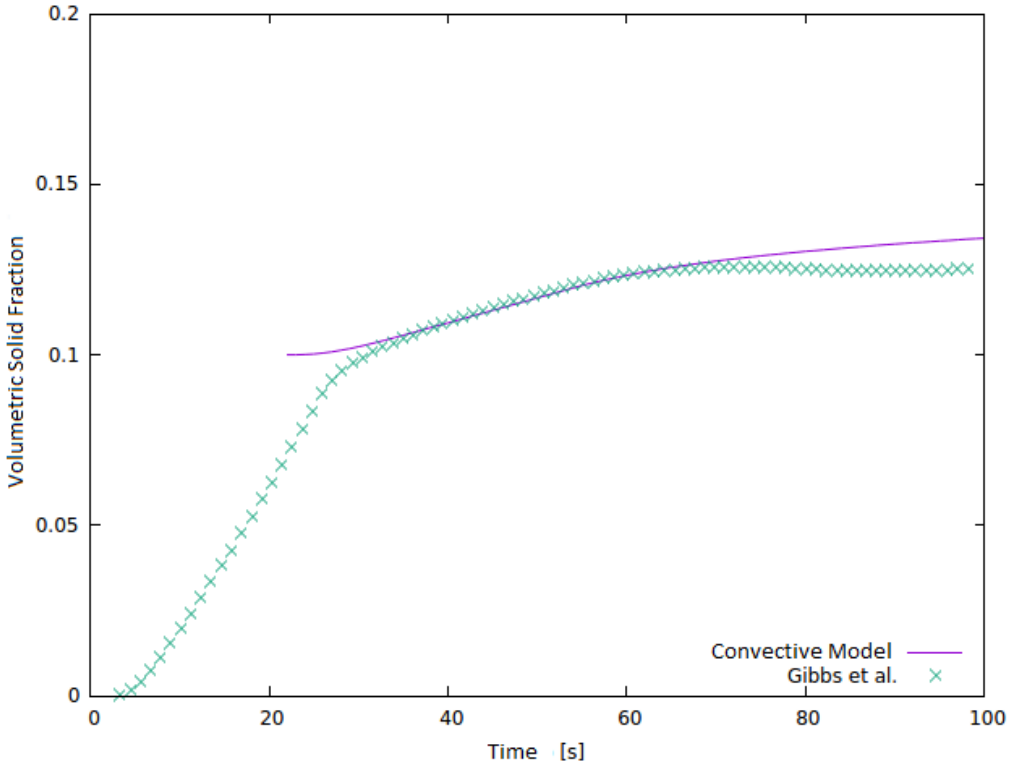

Figure 5: Temporal evolution of the volumetric solid fraction of the convective model in comparison to the reported in (Gibbs *et al.*, 2016).

5. CONCLUSIONS

The numerical model proposed consider the convection in a liquid region between the dendrite arms, therefore, on a microscopic scale. Heat, momentum and solute transfers were considered. Solidification was taken into account in the model by considering solute flow due to segregation from surrounding solid, as well as the release of enthalpy associated with solidification. The causes of asymmetry in the secondary arms of the dendrites, which grow inclined in relation to the thermal gradient. Secondary arms of two neighboring dendrites grow facing and competing each other. When the secondary arms are aligned with isotherms, neither opposite arm is privileged. However, in sloping dendrites relative to the thermal gradient, orthogonal dendritic arms to the primary trunk compete with other opposing arms that grow at different temperatures. Arms that originate at lower temperatures are privileged over arms opposite to higher temperatures. In addition, it was found that although there is a nonuniform distribution of solute, and that this distribution is affected by natural convection, this was not sufficient to significantly affect the growth kinetics of the solid in the studied region. The undercooling distribution was predominantly governed by the temperature field. The convective model also allowed the calculation of a solid fraction that had good agreement with experimental results, although it did not predict a decrease in the solid fraction observed in the experiment. Rather than remelting phenomenon, this behavior was due to buoyancy of dendrites fragments out of measured region. This possibility ws not considered in the present model.

6. ACKNOWLEDGEMENTS

L. M. Bernardo is thankful to CAPES (Coordenação de Aperfeiçoamento de Pessoal de Nível Superior) for partial support of this work.

7. REFERENCES

Beckermann, C., 1997. "Modeling segregation and grain structure development in equiaxed solidification with convection". *JOM*, Vol. 49, No. 3, pp. 13–17.

Clarke, A.J., Tourret, D., Song, Y., Imhoff, S.D., Gibbs, P.J., Gibbs, J.W., Fezzaa, K. and Karma, A., 2017. "Microstructure selection in thin-sample directional solidification of an al-cu alloy: in situ x-ray imaging and phase-field simulations". *Acta Materialia*, Vol. 129, pp. 203–216.

Dantzig, J. and Rappaz, M., 2009. "Solidification: methods, microstructure and modeling".

Gibbs, J.W., Tourret, D., Gibbs, P.J., Imhoff, S.D., Gibbs, M.J., Walker, B.A., Fezzaa, K. and Clarke, A.J., 2016. "In situ x-ray observations of dendritic fragmentation during directional solidification of a sn-bi alloy". *JOM*, Vol. 68, No. 1, pp. 170–177.

Heringer, R., 2004. *Modélisation de la solidification de gouttes atomisées*. Ph.D. thesis, Vandoeuvre-les-Nancy, INPL.

Herlach, D.M., 1994. "Non-equilibrium solidification of undercooled metallic metls". *Materials Science and Engineering: R: Reports*, Vol. 12, No. 4-5, pp. 177–272.

Kurz, W. and Fisher, D., 1989. "Fundamentals of solidification". *Trans. Tech. Aedermannsdorf, Switzerland*, p. 85.

Lipton, J., Glicksman, M. and Kurz, W., 1984. "Dendritic growth into undercooled alloy metals". *Materials Science and Engineering*, Vol. 65, No. 1, pp. 57–63.

OpenFOAM, 2018. "Openfoam v6 user guide: 4.5 solution and algorithm control". CFD Direct. Acessed: 2019-09-05.

Wang, C. and Beckermann, C., 1996. "Equiaxed dendritic solidification with convection: Part ii. numerical simulations for an al-4 wt pct cu alloy". *Metallurgical and Materials Transactions A*, Vol. 27, No. 9, pp. 2765–2783.

8. RESPONSIBILITY NOTICE

The authors are the only responsible for the printed material included in this paper.